

**Amphibious Vehicle Water Egress Modeling and Simulation Using CFD and
Wong's Methodology**

Nathan Tison¹

¹Analytics, CCDC GVSC, Warren, MI

ABSTRACT

A significant challenge for wheel- and propeller-driven amphibious vehicles during swimming operations involves the egress from bodies of water. The vehicle needs to be able to swim to the ramp of a vessel, and then propel itself up the ramp using water propellers and wheels simultaneously. To accurately predict the ability of the vehicle to climb the ramp, it is important to accurately model: (1) the interaction of the flow through the propellers, around the vehicle hull, and away from the ramp; (2) the wheel / ramp interaction; (3) the suspension system spring, damping, and motion-limiting forces, tire deformation and loading characteristics, and wheel and hull motions (both translation and rotation); and (4) the drivetrain power distribution to the wheels. Detailed modeling and simulation of these physics and processes -- such as the wheel, hull, and suspension system motions and force interactions, propeller rotation and resulting flow, etc. -- would be highly computationally expensive. Therefore, to make the water egress problem more tractable to solve, various modeling simplifications -- such as the use of an actuator disc methodology for propeller flow modeling and Wong's terramechanics methodology for the wheel / ramp interaction -- were introduced to facilitate rapid simulation. The integration of a customized six-degree-of-freedom (6DOF) body dynamics solver with a multiphase Volume of Fluid (VOF) computational fluid dynamics (CFD) solver (STAR-CCM+) resulted in an efficient, robust, comprehensive methodology for modeling and simulating amphibious vehicle water egress for various environmental and vehicle characteristics and operational conditions.

Citation: N. Tison, "Wheeled Amphibious Vehicle Water Egress M&S Using CFD and Simplified Vehicle Modeling Methodologies", In *Proceedings of the Ground Vehicle Systems Engineering and Technology Symposium (GVSETS)*, NDIA, Novi, MI, Aug. 13-15, 2019.

1. INTRODUCTION

1.1. Background / Impetus

A significant challenge for amphibious vehicles during swimming operations involves egress from a body of water onto the ramp of a vessel. The

vehicle generally needs to be able to swim to the ramp of a vessel, and then propel itself up the ramp (substrate) using water propellers and wheels simultaneously. To accurately predict water egress, it is important to accurately model: (1) the interaction of the flows through the propellers, around the vehicle hull, and over the substrate; (2) the wheel / substrate interaction; (3) wheel and hull motions (both translation and rotation); (4) the suspension system spring, damping, and jounce-and rebound-limiting forces; (5) tire deformation and loading characteristics; and (6) the drivetrain power distribution to the wheels.

Detailed modeling and simulation of the associated physics and processes would be highly computationally expensive. Therefore, to make the water egress problem more tractable to solve, various modeling simplifications need to be introduced to facilitate rapid simulation. Such comprehensive, simplified modeling methods associated with vehicle egress from a body of water and up a ramp or river bank were not found in the literature.

1.2. Purpose / Scope

A simplified, analytic wheel-substrate interaction modeling approach based upon Wong’s methodology was developed, and simplified propeller, powertrain, suspension, tire, and wheel rotation modeling were incorporated. The resulting simplified vehicle solver was integrated with a computational fluid dynamics (CFD) and six-degree-of freedom (6DOF) body dynamics solver (STAR-CCM+) [2], resulting in an efficient, comprehensive methodology for modeling and simulating amphibious vehicle egress from water to a ramp for various vehicle characteristics and operational conditions. The main content of this paper is organized in terms of the modeling methodology (both the environment and a fictitious vehicle), the simulation methodology, and results.

2. MODELING OF ENVIRONMENT

The environment is comprised by the flow (both water and air) and the substrate (ramp), as in Fig. 1.

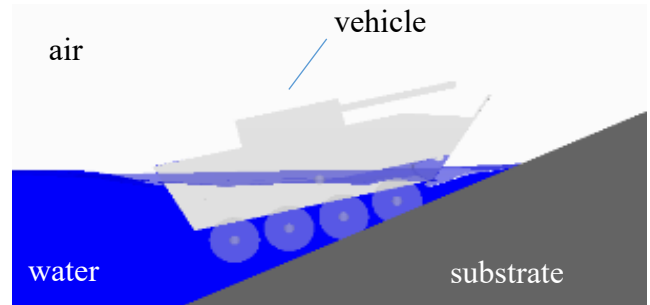


Figure 1: Environmental components

The environmental domain is modeled as in Fig. 2, with a width of 20 m, a length of 40 m, and a height of 30 m.

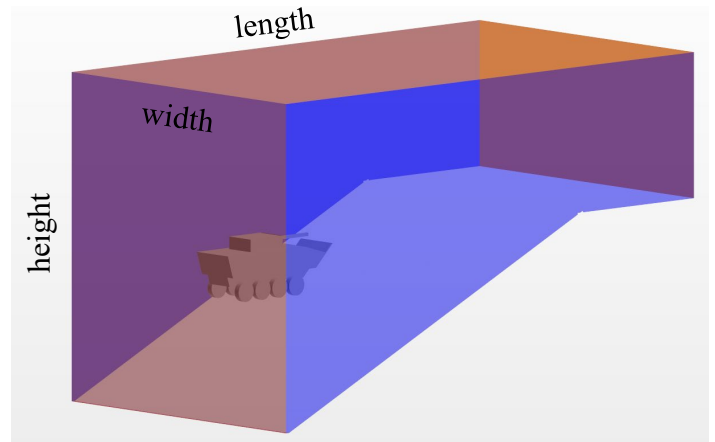


Figure 2: Environmental domain

2.1. SUBSTRATE

The substrate, or ramp, has a sloped portion and a horizontal portion. It is assumed to be hard, and have flow underneath the substrate (ramp). Regarding interaction of the wheels with the substrate, the wheel-substrate overlap d is defined as in Fig. 3, with the overlap direction defined to be normal to the substrate surface and away from the

vehicle. The tractive forces which the hard substrate is able to impart to the wheels is modeled using the coefficient of adhesion attribute, μ , as a constant of proportionality between the wheel-substrate normal and tractive forces. A limiting (or maximum) value, μ_L , can be used to appropriately limit the tractive force for specific limiting-case scenarios (e.g., wet and slippery surfaces). The coefficient of adhesion attribute [1] is specified in terms of a peak coefficient of adhesion value, μ_p , and a sliding coefficient of adhesion value, μ_s .

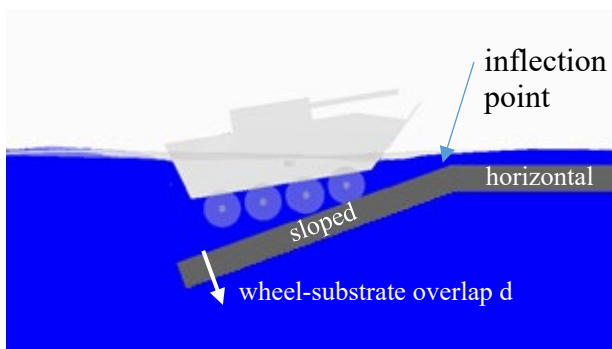


Figure 3: Substrate components

2.2. FLOW

The flow constituents are water and air. The water / air surface tension, density, and viscosity properties are accounted for. The free surface height is specified relative to substrate inflection point.

Various flow constraints are imposed for the flow boundaries shown in Fig. 4. The vehicle boundaries are modeled as moving walls (using 6DOF solving), and the substrate boundaries are modeled as stationary walls; the flow no-slip condition is imposed for all of the wall surfaces. The aft, top, and bottom flow boundaries are modeled as velocity inlets using STAR-CCM+'s "flat wave" condition with zero velocity, turbulent intensity of 1%, and turbulent viscosity ratio of 10. The front boundary is modeled as a pressure outlet using STAR-CCM+'s "flat wave" condition with ambient pressure (accounting for hydrostatic

effects), turbulent intensity of 1%, and turbulent viscosity ratio of 10. The side (right / left) boundaries are modeled as symmetrical, meaning that all of the normal gradients are zero.

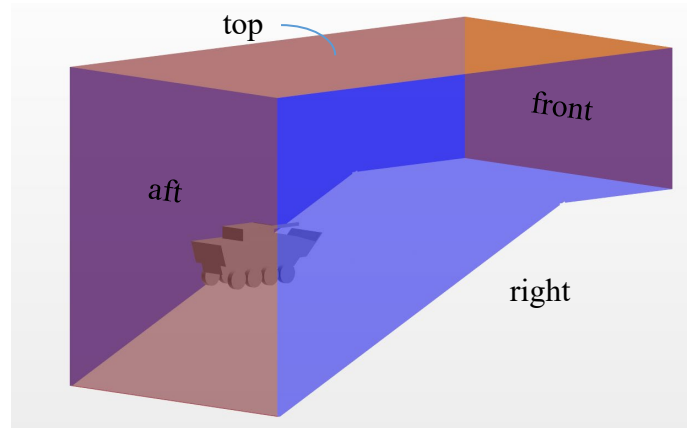


Figure 4: Flow boundaries

The interior constraints are modeled using the Reynolds-averaged Navier-Stokes equations, involving continuity and conservation of momentum. The Realizable k-epsilon two-equation turbulence model and the Volume of Fluid (VOF) multiphase model are also used.

3. MODELING OF VEHICLE

3.1. Overview

The vehicle is comprised by various subsystems which perform various functions (see Fig. 5). The propellers are rigidly attached to hull, and are used to provide water propulsion (thrust) through their interaction with the environmental flow (water). The hull is the dominant inertial component of the vehicle which interacts with the other vehicle components and the environmental flow (via flow drag, buoyancy). The powertrain provides tractive power for the land propulsion running gear (wheels). The suspension transmits forces (and moments) between the hull and each wheel based upon the relative distances and motions. The wheels are attached to the suspension, and are used to provide land propulsion through interaction with the environmental terrain (substrate).

The force interactions among the vehicle subsystems and between the vehicle and its environment, along with the associated motions, are modeled using STAR-CCM+'s flow and 6DOF solving capability [2]. The hull and each of the wheels are modeled independently, allowing their translational and rotational motions to be affected by all of the forces to which each body is subjected to. All of the equations listed below were conceived by the author unless a reference is provided.

3.2. Propellers

The selection of the propeller outer diameter, pitch, blade area ratio, and number of blades – together with the usage of the unducted Wageningen B series shape – results in specified inner (hub) diameter, axial length, and performance characteristics [3]. The associated propulsion characteristics are specified via an “open water” performance data table in terms of dimensionless thrust, torque, and efficiency data over a range of advance ratios. The propellers, depicted in Fig. 5, are modeled using an actuator (virtual) disk method with the thrust and torque distributed in the radial direction based upon Goldstein’s optimum [2].

Other parameters associated with performance include the propeller location (relative to vehicle datum), the area size and location used for

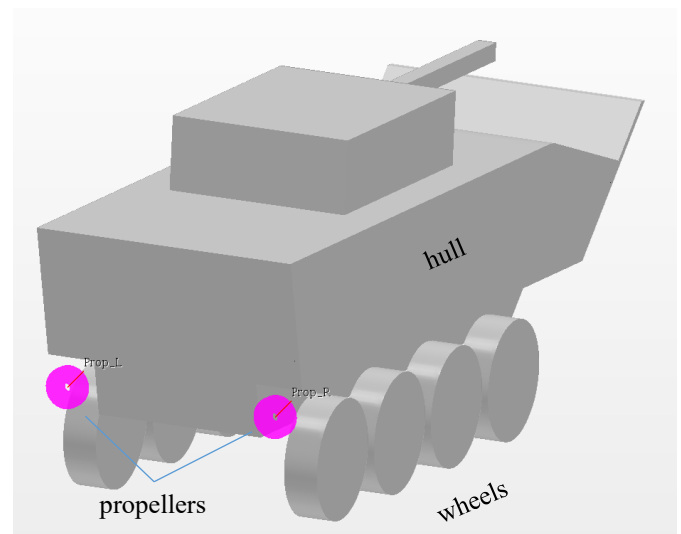


Figure 5: Vehicle subsystems

determination of advance speed, and the propeller rotational speed.

3.3. Hull

Many vehicle-related quantities are defined in terms of the directions associated with the hull (depicted in Fig. 6). The hull-longitudinal (or vehicle-level x-axis) direction extends from aftward to forward. The hull-transverse (or vehicle-level y-axis) direction extends from starboard or right to port or left. The hull-vertical (or vehicle-level z-axis) direction extends from bottom to top.

The hull center of gravity (CG) velocity components are defined in terms of the aforementioned directions, and include the hull-longitudinal component u , the hull-transverse component v (presently assumed to be zero), and the hull-vertical component w .

The hull inertial characteristics include its mass m mass moments of inertia, and CG location. Only the moments of inertia about the cardinal axes – I_{xx} , I_{yy} , and I_{zz} – are accounted for, with the products of inertia neglected; i.e., the vehicle mass

distribution is assumed to essentially be symmetric about the cardinal axes. The hull CG location is placed relative to vehicle datum.

The forces acting on the hull include gravitational, buoyancy, drag (pressure and viscous), and suspension forces.

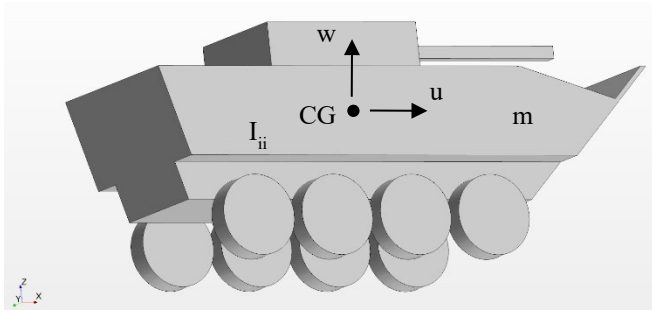


Figure 6: Vehicle hull

3.4. Suspension

Regarding modeling of the suspension system (simply depicted in Fig. 7), various assumptions are made: (1) the suspension system is attached at appropriate points of the wheel assemblies and the hull, such that the suspension forces and moments are reasonably accounted for; (2) the suspension system inertial properties can be appropriately absorbed into those of the wheel assemblies or hull; (3) small portions of the suspension system can be removed to allow hull and wheel movement without hull-suspension-wheel interference, with the removed volume buoyancy accounted for virtually and uniformly distributed among the wheels at the same particular location with respect to each wheel's center of gravity; (4) the suspension system is primarily intended to manage the hull-vertical motion of the wheel assemblies relative to hull, but limited hull-horizontal motion (forward-aftward) is also accommodated; (5) the wheel-hull relative motion is primarily affected by the suspension system through the damping and spring suspension forces; (6) the damping and spring forces are applied to both the wheels and the hull in the appropriate directions, with the hull force direction opposite of that of the wheel (for example,

when the hull is moving forward relative to a wheel's equilibrium position a forward suspension spring force on the wheel is applied and an equal-but-opposite force on the hull is applied, and when the hull is moving upward relative to the wheel an upward suspension damping force on the wheel is applied and an equal-but-opposite force on the hull is applied); (7) the suspension spring and damping parameters are assumed to be identical for the four rear wheels and for the four front wheel; and (8) the suspension cylinder and motion-limiting forces are modeled using spring couplings within the 6DOF solver.

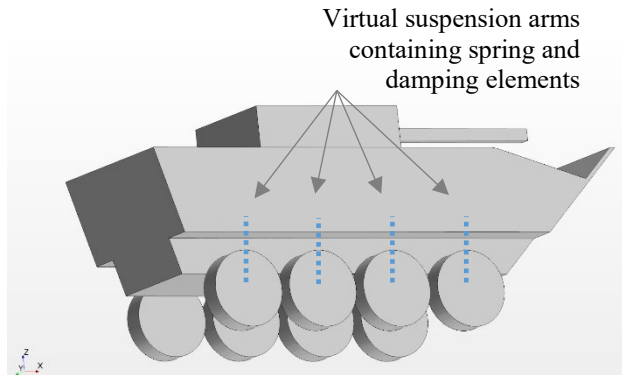


Figure 7: Virtual suspension system

The vertical wheel-hull motion can be described in terms of the suspension stroke length, vertical distance, spring forces, and damping forces. The stroke length can be described in terms of the rebound stroke length, Δz_r , and jounce stroke length, Δz_j . The wheel-hull vertical distance Δz at full rebound, equilibrium, and full jounce conditions can be represented as $\Delta z = 0$, $\Delta z = \Delta z_r$, and $\Delta z = \Delta z_r + \Delta z_j$, respectively.

The vertical spring forces acting on wheel include those associated with the suspension cylinder, rebound limiter, and jounce limiter (e.g., bumpstop), and can be expressed as follows:

$$F_{S, spring, cyl} = \begin{cases} -c_{F_{cyl}, 0} & \text{for } \Delta z \leq 0 \\ -\sum_{i=0}^6 c_{F_{cyl}, i} \Delta z^i & \text{for } 0 < \Delta z \leq (\Delta z_r + \Delta z_j) \\ -\sum_{i=0}^6 c_{F_{cyl}, i} (\Delta z_r + \Delta z_j)^i & \text{for } \Delta z > (\Delta z_r + \Delta z_j) \end{cases}$$

where $c_{F_{cyl}, i}$ is a piecewise-continuous, seven-by-one parameter matrix relating the cylinder spring forces, $F_{S, spring, cyl}$, to Δz ,

$$F_{S, spring, rl} = \begin{cases} -k_{rl} \Delta z & \text{for } \Delta z \leq 0 \\ 0 & \text{for } \Delta z > 0 \end{cases}$$

where k_{rl} is the rebound-limited spring rate constant, and

$$F_{S, spring, jl} = \begin{cases} -k_{jl} (\Delta z - \Delta z_r - \Delta z_j) & \text{for } \Delta z \geq (\Delta z_r + \Delta z_j) \\ 0 & \text{for } \Delta z < (\Delta z_r + \Delta z_j) \end{cases}$$

where k_{jl} is the jounce-limited (bumpstop) spring rate constant.

The vertical damping forces acting on the wheel include those associated with the suspension cylinder, rebound limiter, and jounce limiter (e.g., bumpstop), and can be expressed as follows:

$$F_{S, damping, cyl} = -\beta_{cyl} \Delta w$$

where Δw (first time-derivative of Δz) is the upward velocity of the wheel relative to the hull, and the cylinder damping rate $\beta_{cyl} = \sum_{i=0}^3 c_{\beta_{cyl}, i} \Delta w^i$ and $c_{\beta_{cyl}, i}$ is a piecewise-continuous, four-by-one parameter matrix relating the suspension damping rate to Δw ,

$$F_{S, damping, rl} = -\beta_{rl} \Delta w \text{ for } \Delta z \leq 0$$

where the return-limited damping rate coefficient

$$\beta_{rl} = \begin{cases} 0 & \text{for } \Delta w > 0 \\ \sqrt{2\zeta_{rl} m_w k_{rl}} & \text{for } \Delta w \leq 0 \end{cases}, \text{ and } \zeta_{rl} \text{ is the rebound-limited damping ratio constant,}$$

$$F_{S, damping, jl} = -\beta_{jl} \Delta w \text{ for } \Delta z \geq (\Delta z_r + \Delta z_j)$$

where the jounce-limited damping rate coefficient

$$\beta_{jl} = \begin{cases} 0 & \text{for } \Delta w < 0 \\ \sqrt{2\zeta_{jl} m_w k_{jl}} & \text{for } \Delta w \geq 0 \end{cases},$$

and ζ_{jl} is the jounce-limited damping ratio constant. The composite vertical force accounting for all of the aforementioned forces can then be expressed as:

$$F_{SV} = F_{S, spring, cyl} + F_{S, spring, jl} + F_{S, spring, rl} \\ + F_{S, damping, cyl} + F_{S, damping, jl} + F_{S, damping, rl}$$

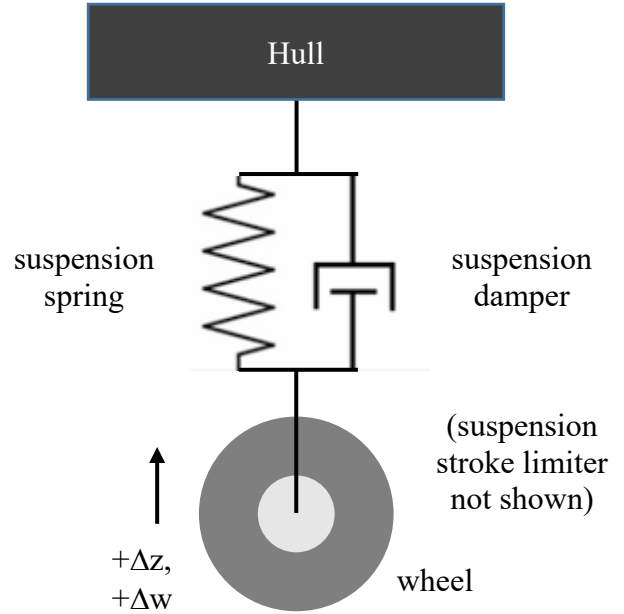


Figure 8: Vertical motion suspension system model

In regards to horizontal motion, the horizontal forces acting on the wheel include those associated with a horizontal motion limiter comprised of a horizontal spring and damper. The spring and damping forces can be expressed as follow:

$$F_{S, spring, hor} = -k_{hor} \Delta x$$

pressure to equilibrium wheel load and m is the total vehicle mass.

- Tire deflection, δ :

$$\delta = \begin{cases} d & \text{for } d \leq \delta_{max} \\ \delta_{max} & \text{for } d > \delta_{max} \end{cases}$$

where δ_{max} is the tire maximum deflection (based on the limits of the available test data).

- Tire effective mass load, m_L :

$$m_L = \sum_{i=1}^3 \sum_{j=1}^3 10^{c_{mL,ij}} p_{inf}^j d^i$$

where $c_{mL,ij}$ is a three-by-four parameter matrix relating tire mass load to deflection and inflation pressure.

- Tire deflected contact length, l_t :

$$l_t = 2\sqrt{D_w \delta - d^2} \sum_{i=0}^2 c_{lt,i} \delta^i$$

(per [1]) where $c_{lt,i}$ is a three-by-one matrix containing parameters relating tire deflected contact length to tire deflection.

- Tire width, b_{ti} :

$$b_{ti} = \sum_{i=0}^2 c_{b,i} \delta^i$$

where $c_{b,i}$ is a three-by-one matrix containing parameters relating tire width to tire deflection.

- Tire contact patch minimum dimension, b : minimum value of l_t and b_{ti} [per 1]
- Tire compression (deflection) half-angle, θ_c :

$$\theta_c = \cos^{-1} \left(1 - \frac{\delta}{R_w} \right) \sum_{i=0}^2 c_{\theta_c,i} \delta^i$$

- Tire deformation motion resistance parameter, ε :

$$\varepsilon = 1 - e^{-\frac{k_e \delta}{h}}$$

where the tire construction parameter k_e is 7 for radial-ply tires and 15 for bias-ply tires [1].

- Tire footprint area, A_{fp} :

$$A_{fp} = c_{A0} \delta^{c_{A1}} = l_t b_{ti}$$

where c_{A0} and c_{A1} are parameters relating the tire footprint area to deflection.

- Tire ground pressure, p_g (over deflected portion):

$$p_g = \frac{F_N}{A_{fp}} \text{ per [1]}$$

- Tire normal spring rate, k_N :

$$k_N = \sum_{i=0}^2 c_{kN,i} p_{inf}$$

where $c_{kN,i}$ is a three-by-one parameter matrix relating the tire normal spring rate to inflation pressure.

- Tire equilibrium deflection, δ_{eq} :

$$\delta_{eq} = \frac{mg}{8k_N}$$

where the number eight appears because the vehicle mass m is assumed to be equally distributed among the eight vehicle tires.

- Tire normal force, F_N :

$$F_N = m_L g + k_N (d - \delta)$$

In the above expression, it can be seen that for tire deflections δ less than δ_{max} , the first term on the right-hand side fully accounts for all of the normal force, and the second term equals zero since δ should be the same value as d for hard substrates.

For δ greater than δ_{max} , the first term on the right-hand side does not fully account for all of the normal force (because δ , which is used to determine m_L , is limited at δ_{max}), and the second term then accounts for the remainder of the normal force associated with tire deflection beyond δ_{max} .

- Tire rolling resistance force, F_R :

$$F_R = 3.581 b_{ti} D_w^2 p_g \varepsilon \frac{(0.0349 \theta_{c,deg} - \sin(2\theta_c))}{2\theta_{c,deg} (R_w - \delta)}$$

where $\theta_{c,deg}$ and θ_c are measured in degree and radians, respectively [1].

- Wheel slip, i [1]:

$$i = 1 - \frac{u}{R_w \omega}$$

where u is the horizontal velocity of the hull.

- Wheel critical slip for hard substrates, i_c [1]:

$$i_c = \frac{F_N}{k_t l_t^2}$$

- Tire tractive force, F_T :

$$F_T = \begin{cases} F_{T^*} & \text{if } F_{T^*} \leq \mu_L F_N \\ \mu_L F_N & \text{if } F_{T^*} > \mu_L F_N \end{cases}$$

where μ_L is a limiting adhesion coefficient value and

$$F_{T^*} = \begin{cases} 0.5k_t l_i^2 i & \text{for } i \leq i_c \\ F_N \left[\mu_p \left(1 - \frac{\mu_p F_N}{2k_t l_i^2 i} \right) \frac{(1-i)}{(1-i_c)} + \mu_s \frac{(i-i_c)}{(1-i_c)} \right] & \text{for } i > i_c \end{cases}$$

which involving a customized transition from critical slip ($i = i_c$) to complete slip ($i = 1$) partially based upon Wong’s methodology [1].

- Tire tractive torque, T_T :

$$T_T = \begin{cases} T_{T^*} & \text{if } F_{T^*} \leq \mu_c F_N \\ T_{T^*} \left(\frac{F_N \mu_L}{F_{T^*}} \right) & \text{if } F_{T^*} > \mu_L F_N \end{cases}$$

where $T_{T^*} = (R_w - \delta) F_T$

- Wheel rotational speed, ω :

$$T_P + T_F - T_T = I_{w,r} \frac{d\omega}{dt}$$

where ω is determined by integrating the above equation with respect to time and T_F is the torque on the wheel resulting from flow forces as determined from the CFD solver.

- Wheel equivalent speed, v_{eq} :

$$v_{eq} = \omega (R_w - \delta_{eq})$$

3.6. Powertrain

Regarding the vehicle powertrain, only the torque which it provides to the wheels is modeled. The available powertrain torque for each wheel, $T_{AP,i}$, can be expressed as:

$$T_{AP,i} = \sum_{j=0}^3 \frac{C_{APF,j}}{8} v_{eq,i}^j (R_w - \delta_{eq})$$

where: i identifies the wheel; v_{eq} is the wheel equivalent speed; $C_{MPF,j}$ is a piecewise-continuous, four-by-one parameter matrix relating the maximum available vehicle powertrain force to v_{eq} based on vehicle tractive force (or torque or power) and speed data involving specified vehicle mass, tire deflections, substrate grade, and optimum slip

conditions; and the number eight appears because the total vehicle powertrain force (per the test data) was assumed to be distributed equally among the eight wheels.

The maximum powertrain torque available for all wheels, T_{AP} , can be expressed as:

$$T_{AP} = \sum_{i=0}^8 T_{AP,i}$$

The powertrain torque available for all of the wheels, T_{AP} , is distributed among the wheels by assuming that all of the wheels are “locked” together, such that they all share the same rotational speed. Torque is applied as required – positively or negatively – in order to have all of the wheels spin with the same rotational speed (based on the assumption that powering / braking torque can be distributed appropriately). The distribution of the available torque is limited, however. Powertrain torque is not applied to a given wheel if that wheel’s rotational speed has already surpassed an upper limit (ω_{lim}) or if that wheel’s slip is less than a target slip value (i_{tar}); in such cases, only the torque loads (substrate, flow) are applied to the wheel.

4. SIMULATION

The simulation methodology used can be described in terms of the associated solver utilization, execution, data passing, initialization, and time-marching.

4.1. Solver Utilization

Two solvers are used to incorporate the previously described modeling methodology and to accomplish the simulations: a “flow / 6DOF” solver and a “vehicle” solver.

The “flow / 6DOF” solver involves modeling of the: (1) hull / wheel motions / forces and suspension spring coupling models (“6DOF”); and (2) flow dynamics, including the propeller-, hull-, and substrate-flow interactions (“flow”). To accomplish this, a commercial-off-the-shelf (COTS) CFD solver – STAR-CCM+ [2] – is used

to simulate the flow and hull / wheel motions and forces based upon its unsteady Reynolds-Averaged Navier-Stokes (uRANS) equations, Volume of Fluid (VOF) multi-phase flow modeling method, six degree of freedom (6DOF) rigid body motion modeling, and overset meshing capabilities. A “two-layer all y^+ wall treatment” is used for the near-wall prism layer cells, and hull and wheel flow cells allowed to be no larger than 50mm. Overset meshing (or “Chimera” or overlapping meshing) is used to allow the hull and wheel meshes to move relative to one another as well as the environment mesh, and overlap each other in such a way that the governing physical equations can still be solved.

The “vehicle” solver involves the modeling of the suspension, wheels, hull, and powertrain characteristics and interactions. It is contained within the STAR-CCM+ Java run script.

4.2. Solver Execution

A STAR-CCM+ Java run script is used to control both the flow / 6DOF solver (STAR-CCM+) as well as the vehicle solver (which is embedded within the run script), and facilitate the passing of data back and forth. Department of Defense Supercomputing Resource Center (DSRC) resources – namely, Thunder, Mustang, Centennial, Onyx, Topaz, Gaffney, and Koehr – are used to run the solvers.

4.3. Solver Data Passing

The data passed between the solvers occurs as depicted in Fig. 9.

4.4. Solver Initialization

The solver initialization involves two main steps: parameter setting and variable initialization. The parameters set, based on user input, include geometry parameters (substrate angle), mesh parameters (refinement region boundaries and mesh sizing), simulation parameters (first order discretization for stability purposes, 2 ms time step), and environmental and vehicle model

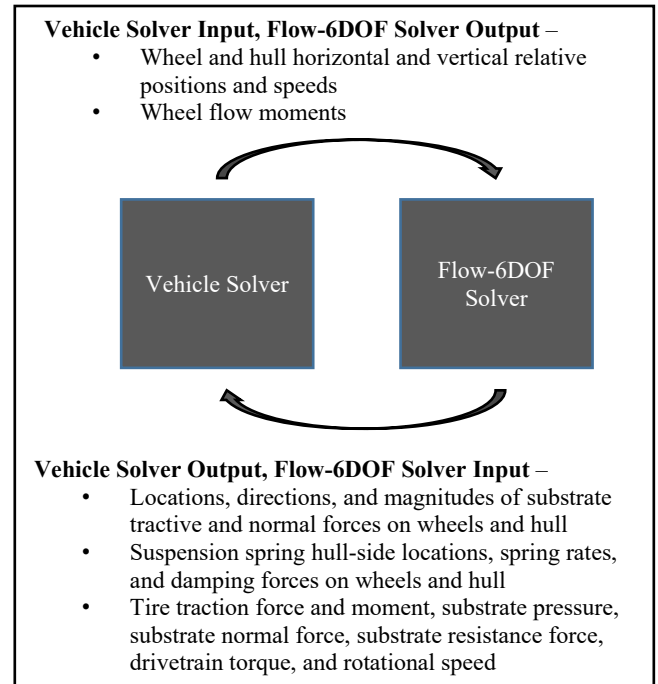


Figure 9: Solver data passing schematic

parameters: hull inertial properties (mass, mass moments of inertia, CG location); powertrain maximum available torque and torque distribution method; substrate angle, tractive properties, and limiting coefficient of adhesion; wheel / tire inertial properties, tangential stiffness, section height, and construction parameter [1]; and suspension virtual buoyancy points, rebound limit, jounce limit, and horizontal motion spring and damping rates .

The variable initialization involves: (1) the tire inflation pressure (based upon the equilibrium mass load of the vehicle); (2) tire normal deflection spring rate (based upon the tire inflation pressure); (3) tire equilibrium deflection (based upon the vehicle mass and the tire normal spring rate); (4) hull / wheel initial positions and velocities (based upon user input); (5) wheel initial rotational speeds (based on the initial vehicle speed and the target slip); (6) propeller sizing and placement (based upon user input); and (7) flow velocity and pressure.

4.5. Solver Time-Marching

The solver time-marching can be described in terms of the vehicle solver and the flow / 6DOF solver. For the vehicle solver, three main sections are executed for each vehicle wheel: a preliminary section, a middle section, and a final section. The vehicle solver preliminary section involves: (1) inputting of the hull and wheel positions and speeds (both horizontal and vertical), along with the wheel flow moments; (2) determination of the wheel-substrate normal distances and outputting of the force locations (within the tire deflection planes) and appropriate directions (parallel or normal to the substrate surface, as appropriate), based upon the CG location of the wheel relative to the substrate inflection point; (3) outputting of the buoyancy force for the missing suspension geometry based upon the CG location of the wheel relative to the free surface; and (4) computation of wheel slip i based upon the rotation speed associated with the last time step.

The vehicle solver middle section first involves determination of whether or not wheel / substrate contact is occurring. If contact is not occurring, the tire normal and tractive forces are set to zero. If contact is occurring, multiple steps – organized in terms of preliminary, middle, and final steps – are accomplished. The preliminary steps involve determination of tire contact patch length, width, minimum patch dimension, deformation motion resistance parameter, compression (deflection) half-angle, and footprint area. The middle steps involve setting the tire deflection to be equal to the wheel-substrate overlap, and determination of effective tire load, tire normal force, wheel critical slip, tire tractive force, tire tractive torque, ground pressure, and resistance force. The final step involves modification of the tire tractive force and tractive torque based on the ceiling coefficient of adhesion.

The vehicle solver final section involves: (1) determination of the wheel-hull relative distances and velocities, and of the wheel equivalent speed, maximum drivetrain torque, flow torque, total

(flow and substrate) torque load; (2) determination / outputting of the suspension hull-side spring locations, spring rates, damping rates and forces (both wheel and hull), and of the wheel rotational speed based upon powertrain torque distribution method; (3) outputting of the substrate normal and tractive forces on wheel to the Flow-6DOF solver; and (4) control of propeller operation. When wheel-substrate contact does not occur, the propellers are operational if the vehicle speed is below the land speed target, and inoperational if the vehicle speed is above the land speed target. When wheel-substrate contact does occur, the propellers are operational if the vehicle speed is below the water speed target and the propellers are below the free surface, and inoperational if the vehicle speed is above the water speed target.

For the flow-6DOF solver, the following two main steps are executed. From the vehicle solver, the vehicle parameters, suspension hull-side spring locations and spring rates, suspension damping forces, substrate damping forces, substrate normal and tractive forces on wheel, and wheel rotational speeds are inputted into the flow-6DOF solver. Using the current flow field – along with the inputted forces and other values – the flow-6DOF solver determines the vehicle hull translation / rotation and new orientation, the wheel translations and new positions, and the new flow field and the new flow forces / moments; the hull and wheel positions and speeds – both horizontal and vertical – are outputted to the vehicle solver, along with the wheel flow moments.

5. RESULTS

Simulations of various amphibious vehicle egress scenarios using the proposed methodologies were performed using the values of the parameters listed below in Table 1.

Class	Entity	Sub-Entity	Parameter					
			Name	Symbol	Domain / Comments	Setting / Value	Units	
Modeling	Environment	Flow	Water free surface location	-			m	
			Water density	-		999.98	kg/m ³	
			Water viscosity	-		1.51E-03	kg/m-s	
			Air density	-		1.18415	kg/m ³	
			Air viscosity	-		1.86E-05	kg/m-s	
			Water-air surface tension	-		0.072	N/m	
		Substrate	Peak coefficient of adhesion	μ_p		0.6	-	
			Sliding coefficient of adhesion	μ_s		0.4	-	
			Limiting coefficient of adhesion	μ_L		0.8	-	
			Substrate angle	-		25	degrees	
			Objective speed in water	-		5	mph	
			Objective speed on substrate	-		8	mph	
			Datum longitudinal position	-	Rel. to center of front-axel	-1814.4	mm	
			Datum transverse position	-	axis	0	mm	
	Datum vertical position	-		1104.4	mm			
	Vehicle	General	Center of gravity longitudinal position	CG _x	Relative to vehicle datum	0	mm	
			Center of gravity transverse position	CG _y		0	mm	
			Center of gravity vertical position	CG _z		0	mm	
			Mass	m		30000	kg	
			Hull	Moment of inertia about longitudinal axis	I _{xx}	Rotational axis goes through CG	6.78E+04	kg-m ²
				Moment of inertia about transverse axis	I _{yy}		2.04E+05	kg-m ²
		Hull Moment of inertia about vertical axis		I _{zz}		2.07E+05	kg-m ²	
		Center of gravity longitudinal position		-		0	mm	
		Center of gravity transverse position		-		0	mm	
		Center of gravity vertical position		-	Relative to vehicle datum	-7.36E+01	mm	
		Longitudinal position		-		-3733.4	mm	
		Propeller	Transverse position	-		+/-1187.5	mm	
Vertical position			-		-450	mm		
Inner radius	-			50	mm			
Outer radius	-			225	mm			
Axial length	-			100	mm			
Rotational speed	-			2000	rpm			
Wheel	Tire tangential spring rate		k _t		4.00E+06	N/m ²		
	Tire section height	h		0.33575	m			
	Tire construction parameter	k _e		7	-			
	Tire maximum deflection	d _{max}		140	mm			
	Wheel radius	R _w		6.72E+02	mm			
	Wheel target slip	i _{tar}		2.50E-01	-			
	Wheel rotational moment of inertia	I _{w,r}		7.50E+01	kg-m ²			
	Assembly moment of inertia about long. axis	I _{w,xx}	Not used	3.31E+01	kg-m ²			
	Assembly moment of inertia about trans. axis	I _{w,yy}		9.97E+01	kg-m ²			
	Assembly moment of inertia about vert. axis	I _{w,zz}		1.01E+02	kg-m ²			
	Wheel rotational speed upper limit	ω_{lim}		5.00E+02	rpm			
	Wheel assembly mass	m _w		2.34E+02	kg			
	Wheel assembly missing volume	-		6.25E-04	m ³			
	Suspension	Jounce stroke length	Δz_j		1.50E+02	mm		
Rebound stroke length		Δz_r		1.50E+02	mm			
Torque distribution ratio limit		-		0.375	-			
Simulation	General	Time step	-		2	ms		
		Flow-6DOF	Discretization order	-		1	-	
	Vehicle	Initial speed	-		5	mph		
		Initial suspension stroke distance	-		1.50E+02	mm		

Table 1: Results general parameters

For this initial study, the only performance metric considered was whether or not the vehicle could fully climb up the ramp. An example plot of flow velocity magnitude contours – on a plane bisecting the left propeller – can be seen in Fig. 10, with a black line showing air / water interface. Higher velocity regions can be noticed in the vehicle wake, at the vehicle bow, and at the vehicle propeller (especially).

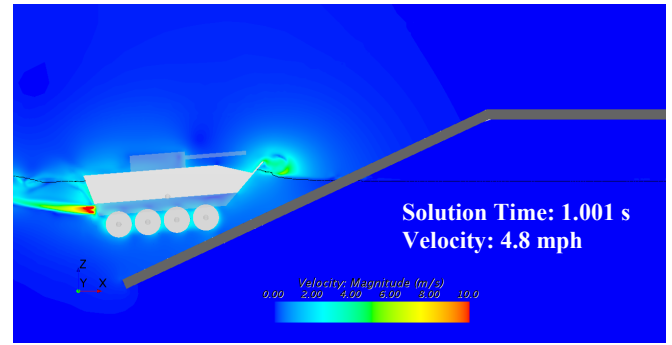


Figure 10: Example flow velocity contour

A corresponding air / water free surface plot – with white color representing air and blue color representing water – is shown in Fig. 11. In these plots, the vehicle velocity (in the longitudinal direction) is also displayed.

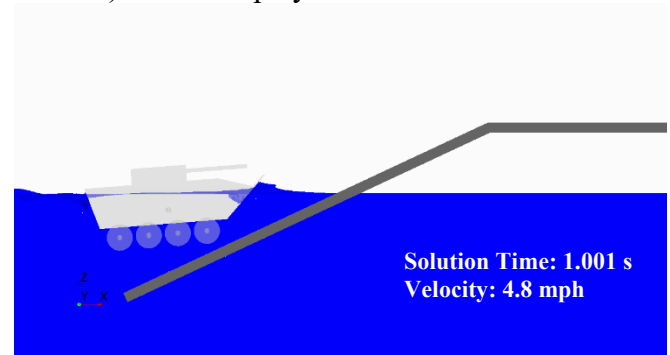


Figure 11: Example free surface plot

The free surface results for a baseline case involving a substrate angle of 25 degrees with respect to horizontal are shown in Fig. 12. It can be seen here that the vehicle is predicted to essentially be able to fully climb the ramp, as evidenced by the front wheels having cleared the substrate point of inflection and the vehicle still having significant forward velocity.

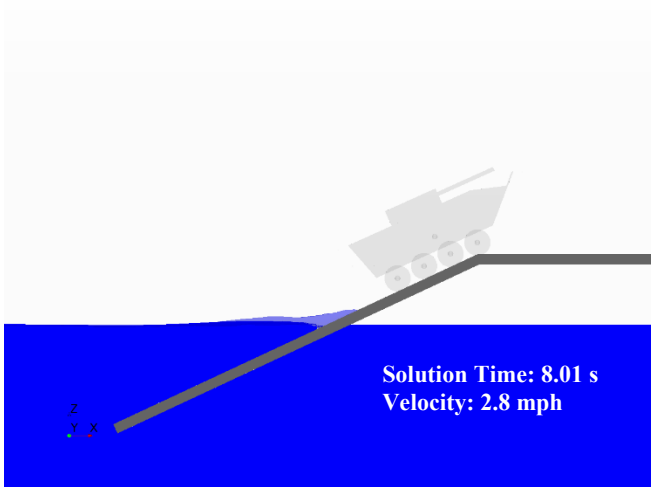


Figure 12: Results for baseline case

5.1. Effect of Increased Substrate Angle

For the case where the ramp angle is increased from 25 to 35 degrees (and all other characteristics remaining the same), the vehicle is predicted to not be able to fully climb the ramp. In Fig. 13, the greatest extent to which the vehicle was able to climb the ramp – along with the associated velocity of zero (just before the vehicle started to slide down the ramp) can be seen.

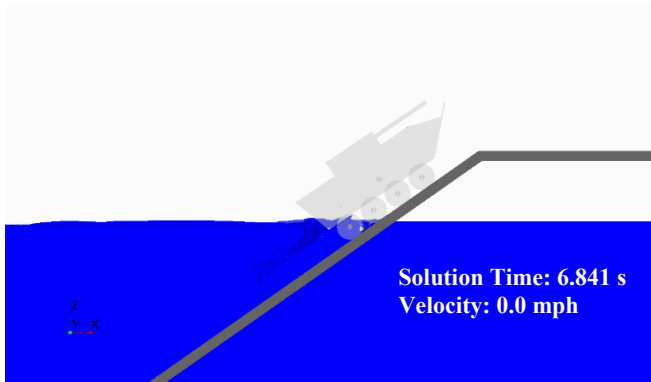


Figure 13: Results for substrate angle of 35 degrees

5.2. Effect of Reduced Powertrain Torque

For the case where the available powertrain torque is cut in half (and all other characteristics remaining the same), the vehicle is again predicted to not be able to fully climb the ramp. In Fig. 14, the greatest extent to which the vehicle was able to climb the ramp – along with the associated velocity of zero (just before the vehicle started to slide down the ramp) can be seen.

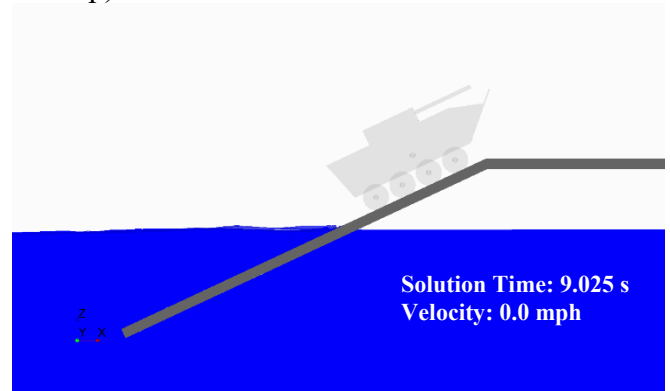


Figure 14: Results for reduced powertrain torque

6. CONCLUSION

6.1. Summary

A simplified, analytic wheel-substrate interaction modeling approach based upon Wong's methodology was developed, and simplified propeller, powertrain, suspension, tire, and wheel rotation modeling were incorporated. The resulting simplified vehicle solver was integrated with a computational fluid dynamics (CFD) and six-degree-of freedom (6DOF) body dynamics solver (STAR-CCM+), resulting in an efficient, comprehensive methodology for modeling and simulating amphibious vehicle egress from water to a ramp for various vehicle characteristics and operational conditions. Simple studies were performed to demonstrate the method's capability as it relates to predicting the ability of a vehicle to egress from water and successfully climb a ramp.

6.2. Future Work

The following areas of study will be pursued: (1) transverse water current; (2) soft substrate capability development using an analytical (Bekker-based) method; (3) soft substrate capability development using empirical (cone-index-based) method; and (4) validation.

7. REFERENCES

- [1] J. Y. Wong, *Theory of Ground Vehicles*. Hoboken, NJ: John Wiley & Sons, Inc., 2008.
- [2] Siemens Technical Staff, *STAR-CCM+ User Guide*, Siemens, 2019.
- [3] M. W. C. Oosterveld and P. van Oossanen, "Further Computer-Analyzed Data of the Wageningen B-Screw Series", *International Shipbuilding Progress*, vol. 22, no. 251, pp. 251-262, 1975.